Nanomaterials and Nanotechnology

OPEN ACCESS
ARTICLE

Edge-sensitive Semiconducting Behaviour in Low-defect Narrow Graphene Nanoribbons

Regular Paper

Syota Kamikawa[1], Taisei Shimizu[1], Yuko Yagi[1] and Junji Haruyama[1,*]

1 Faculty of Science and Engineering, Aoyama Gakuin University, Sagamihara, Kanagawa, Japan
* Corresponding author E-mail: J-haru@ee.aoyama.ac.jp

Received 12 Jan 2014; Accepted 5 Mar 2014

DOI: 10.5772/58466

Abstract Low-defect graphene nanoribbons (GNRs) derived from the unzipping of carbon nanotubes have exhibited large energy band gaps (transport gaps), despite having widths in the order of ~100 nm. Here, we report on the unique semiconducting behaviour of very narrow, low-defect GNRs, with widths of less than 20 nm. Narrow GNRs are highly resistive, and additional annealing is required to reduce their resistivity. The GNRs display ambipolar rather than evident semiconducting behaviour (p- and n-types), exhibiting normalized I_{on}/I_{off} as great as ~10^6 (close to those in a few nm-order-width GNRs) and which are very sensitive to the atmosphere and the termination of the GNRs' edges by foreign atoms (hydrogen for n-type and oxygen for p-type). It is also revealed that the activation energy (E_a ~35 meV) estimated from the temperature dependence of the minimum conductance is smaller than those in ~100 nm width GNRs. The observed sharp conductance peak on back-gate voltage (V_{bg}) dependence and its strong correlation with the E_a value suggest the presence of possible resonant tunnelling through shallow impurity levels with the small E_a introduced by the edge terminations by foreign atoms, which provides the observed unique behaviour, including the high I_{on}/I_{off}. An energy band gap as large as ~215 meV is also confirmed from the I_{off} voltage region on V_{bg}. These narrow GNRs must open the door to large-scale graphene integration circuits based on CMOS-like behaviour.

Keywords Graphene, Nanoribbon, Edge, Semiconducting Behaviour, Impurity Level, Resonant Tunnelling

1. Introduction

Graphene has attracted considerable attention due to its unique electronic properties [1, 2]. In particular, it is important to realize well-controlled semiconducting behaviours in graphene to enable its future use in large-scale integration (LSI) circuits because pristine graphene is a semimetal (a gapless semiconductor). At least two effective approaches have been used for this: (1) the formation of bilayer graphenes [3-7] and (2) the formation of graphene nanoribbon (GNR; pseudo one-dimensional (1D) strip-lines of graphenes) structures with armchair-type edges [8-28].

For GNRs, the quasi-1D confinement of carriers and the presence of armchair edges induce an intrinsic energy gap in the single-particle spectrum [22-24]. Given this, we have reported the fabrication of field-effect transistors (FETs) using low-defect GNRs derived from a non-lithographic method (i.e., the unzipping of carbon nanotubes (CNTs) with the air-blow method and three-step annealing [15]). In the low-defect GNRs, even with a width as wide as ~75 nm, we confirmed an intrinsic energy band gap as large as ~50 meV, which was seven-times greater than that in lithographically-defined high-density-defect GNRs, as well as some semiconducting behaviours.

On the other hand, other groups have reported on the semiconducting behaviours of narrower GNRs (width <40 nm) [18-20]; e.g., p-type semiconducting behaviour with on/off ratios of I_{sd} upon V_{bg} change (I_{on}/I_{off}) up to 10^6 in ~2 nm-wide GNRs, changing from p-type to n-type behaviours with $I_{on}/I_{off} \sim 10^5$ in similar ~5 nm-wide GNRs with electron doping in an ammonia atmosphere, and the evident single-electron charging effect (the so-called artificial Kondo effect) in CNT-derived smooth-edge GNRs with sub-10 nm widths [18]. Extremely large magnetoresistance arising from the unique symmetry of band gaps is also predicted in GNRs for the generation of highly spin-polarized current [26]. Even fast and reliable DNA-sequencing devices are predicted, utilizing the distinct conductance behaviours of GNRs [27].

The appearance of such semiconducting behaviour has been understood based on the shifting of the Fermi level (E_F) - which is sensitive to carrier doping via the GNR edges [29-34] - through the 1D electronic density of states (EDOS) with van Hove singularities (VHSs). However, the correlation of semiconducting behaviour with the presence of impurity levels introduced via edge termination by foreign atoms has not thus far been experimentally reported, although there are many theoretical reports (particularly as regards calculating resonant tunnelling via impurity levels originating from edge termination by foreign atoms) [35-38]. In the present study, we observe this correlation in low-defect narrow GNRs (<~20 nm width). Narrow GNRs are highly resistive, and additional annealing is required to reduce their resistivity. The GNRs show not ambipolar (i.e., charge-neutral points) but rather evident semiconducting behaviours (like p- and n-types) exhibiting normalized I_{on}/I_{off} as great as ~10^6, which are highly sensitive to atmospheres and the termination of the GNRs' edges by foreign atoms [29-34]. We noticed the presence of a conductance peak at the low voltage region and discussed its correlation with resonant tunnelling via impurity levels, which can realize the observed semiconducting behaviours.

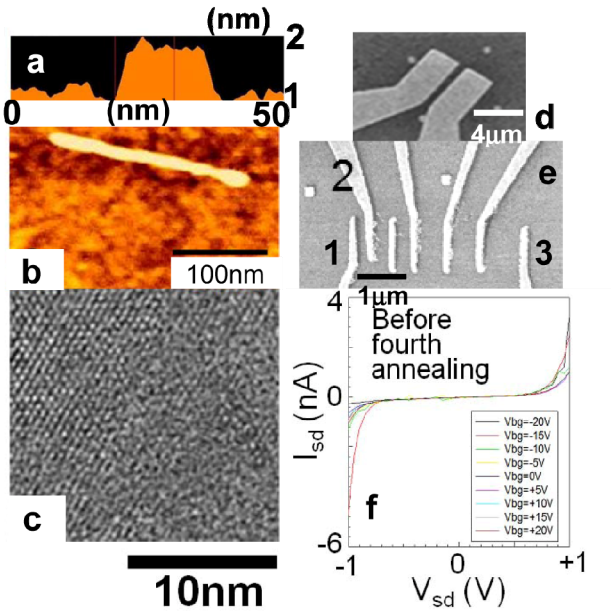

Figure 1. a Cross-sectional atomic force microscope (AFM) image of a narrow GNR with a width of ~20 nm. **b,** its top-view image. For (a), one point of the GNR shown in (b) was exhibited. The top portions of the GNR are mostly flat, without showing any curvature. **c,** The observation of a hexagonal graphene lattice in high-resolution transmission electron microscope (HRTEM) images before the three-step annealing. **d, e,** Scanning electron microscope (SEM) images of FET electrode patterns with Ti/Au (15 nm/100 nm) for short (d, 600 nm) and long (e, 3600 nm) GNRs. The inter-electrode distance is 400 nm for (d), and 400 nm between electrodes 1 and 2 and 3,000 nm between electrodes 1 and 3 for (e). **f,** Typical drain current (I_{sd}) vs. drain voltage (V_{sd}) relationship of the sample shown in Figs. 1b and 1d at 1.5 K before performing the fourth annealing.

2. Sample fabrication and characterization

The GNRs fabricated in the present study were prepared by oxidization and the longitudinal unzipping of multi-walled CNTs, basically following our previous methods [15-17]. As a significant difference, in order to separate the entangled as-grown narrow GNRs and obtain suitable rectangle-high aspect-ratio structures of individual GNRs on the SiO_2 substrate, an air gun or conventional heat dryer was used. Air flow from either of these was applied to the H_2O droplet containing the as-grown GNRs, and the air flow direction was changed every 60 s a total of ~80 times. The strength of the air flow was tuned by controlling the distance between the droplet and the air gun. The droplet was moved around on the substrate by this action and the entangled as-grown GNRs were separated. (Figs. 1a and 1b). Next, the substrate surface was dried at 400 °C in high vacuum (10^{-6} Torr).

Subsequently, three-step annealing was carried out following our previously-described protocol [15]. As the fourth step, annealing was performed under high vacuum (10^{-6} Torr) at 700 °C immediately after the formation of the

metal electrodes. This temperature is critical to ensuring that no damage occurs to the Au/Ti metal electrode.

The low-defect concentration of the fabricated GNRs was confirmed by the observation of a high-intensity G band and a low-intensity D band, along with a low-intensity 2D band in the Raman spectrum obtained after the annealing as well as the case in [15]. The D-band peak becomes slightly larger than those in previous, wider GNRs [15], due to the induced influence of the residual edge disorder in narrow GNRs. The absence of defects was also inferred from the observation of a clear hexagonal graphene lattice with small-amount defects in high-resolution transmission electron microscope (HRTEM) images (Figure 1c). Although some defects still remain - because it was observed before annealing - it shows a much better HRTEM image compared with lithographically fabricated GNRs. The reduction of the D peak height after annealing suggests the disappearance of these defects.

Using these low-defect narrow GNRs, we fabricated FETs with short-length GNRs (600 nm length: Figure 1d) and long GNRs (3,600 nm length: Figure 1e). Each electrode - including the back gate - is composed of Ti/Au and the electrode pads were placed on SiO_2.

3. Electrical properties and discussion

3.1 Basic property and 4th annealing

Figure 1f shows the typical drain current (I_{sd}) values as a function of the drain voltage (V_{sd}) of an FET fabricated using a short-length GNR (Figure 1d) as the current channel at a temperature (T) of 1.5 K. The current amplitude is small, with the presence of a strong zero-bias conductance (G_0) anomaly (a voltage width of ΔV_{SD} ~±1 V even at a back-gate voltage (V_{bg}) of ±20 V). We observed that most of the fabricated narrow GNRs (width ~20 nm) were highly resistive (i.e., a small magnitude of I_{sd}) with strong G_0 anomalies even after the three-step annealing [15] when compared with our previously-fabricated wide GNRs (width >75 nm).

Although the width of the narrower GNRs is less than ~1/3 of the width of the wider GNRs, the resistivity is at least 10-times larger. This result cannot be understood by the conventional relationship of resistivity vs. the width of the GNRs, which is an inversely proportional relationship. Moreover, the G_0 anomaly cannot be attributed to the single-electron charging effect [15] (see Author's note).

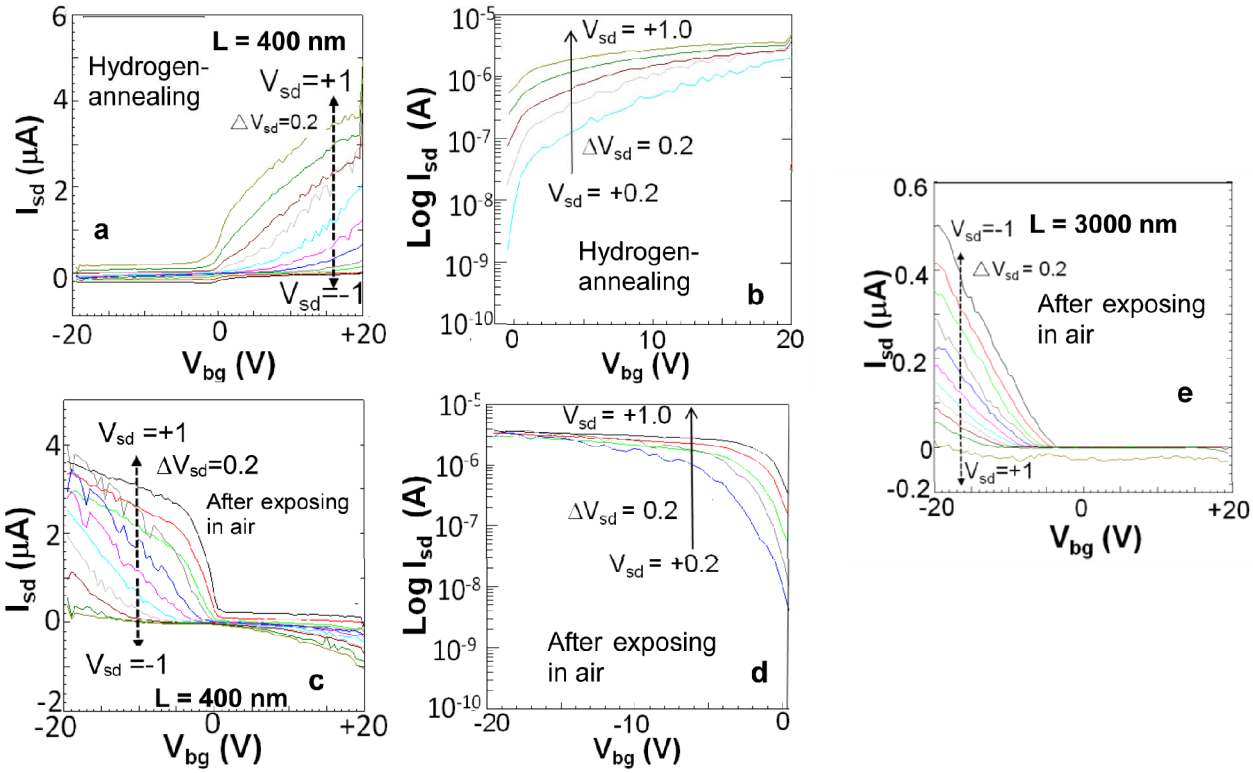

Figure 2. a, b, Drain current (I_{sd}) vs. back-gate (BG) voltage (V_{bg}) curves at 300 K for the sample shown in Figure 1b (400 nm length) with *H*-terminated edges. The significant I_{SD} increase observed only in the $+V_{bg}$ region suggests n-type semiconductive (i.e., electron-dominant) transport. Owing to insufficient isolation between the BG and source pads, leakage current remains even at V_{sd}=0. In (b), the y-axis represents the logarithmic scale of the values of I_{sd} shown in the $+V_{bg}$ region of Figure 2a. **c, d**, I_{sd} vs. V_{bg} curves at 300 K for the sample corresponding to Figure 2a after exposure to atmospheric air for two weeks at room temperature. **e,** I_{sd} vs. V_{bg} curves at 300 K for an *O*-terminated long sample corresponding to Figure 1e (length of 3,000 nm) obtained after exposure to atmospheric air, similar to Figure 2c.

However, after we carried out the fourth annealing process under high vacuum at 700 °C immediately after the formation of the metal electrodes (methods), the amplitude of I_{sd} exhibited a significant recovery. This implies that the previously-observed high resistivity (Figure 1f) was due to poor interface contact between the metal electrode and the narrow GNRs. After the fourth annealing, further deoxidization from the GNR can at least occur. The GNRs present were fabricated by the unzipping of CNTs by the oxidation of defects. Thus, after the formation of the GNRs, oxygen (O)-atoms remained. Here, even if the number of the remaining O atoms is very small and mostly the same between the wide and narrow GNRs after the three-step annealing, the resistivity at the interface of the electrodes/GNR is significantly affected only in the narrow GNRs because the ratio of the O atoms/GNR width is larger in the narrow GNRs. This can result in larger interface resistivity. After the fourth annealing, O atoms beneath the electrodes move and can be excluded further, resulting in low interface resistivity.

3.2 Semiconducting behaviours on edge termination

Figure 2a shows the typical I_{sd} vs. V_{bg} curve for the sample with a 600 nm length at T = 300 K, after the fourth annealing. The I_{sd} value is significantly enhanced by the fourth annealing step. In the V_{bg} range between ±20 V, the device does not exhibit ambipolar behaviour but instead evident n-type semiconductor behaviour, where I_{sd} drastically increases only when the applied V_{bg} is positive. This behaviour is qualitatively consistent with the behaviour reported in previously fabricated carrier-doped GNRs with sub-10 nm-widths and graphene nanomeshes with an inter-pore distance (i.e., GNR width) of ~20 nm [18-20]. However, an I_{on}/I_{off} ratio as high as ~10^4 is observed at V_{sd} = 0.2 V, even with the leakage I_{sd} at V_{sd} = 0 V (Figure 2b with the y-axis representing the logarithmic-scale values of the I_{sd} value in Figure 2a). This I_{on}/I_{off} ratio is 10^3 times greater than those observed in previously fabricated ~20 nm-width GNRs [19, 30]. Surprisingly, this value is equal to ~10^6 as reported in 2 nm-wide GNRs, when the I_{on} is normalized for the GNR width (i.e., normalized I_{on} ~ 200 μA/μm = I_{on} ~ 4μA/20 nm (Figure 2a) × 1μm/20 nm) [20].

As mentioned above, the observed semiconducting behaviour that does not exhibit transport gaps (or charge neutrality points, band gaps) in sub-10 nm GNRs has been understood only by the shift in E_F through the VHSs of 1D EDSs caused by edge carrier doping. This shift can also produce large I_{on}/I_{off} values due to a significant increase in EDOS caused by the E_F shifting along a VHS. However, in the presence 20 nm-GNRs, no evident 1D EDOS exists because the GNR width is greater than 10 nm and, hence, the observed semiconducting behaviour with the extremely large normalized I_{on}/I_{off} values of ~10^6 cannot be fully understood by this model alone. We discuss our model (considering E_F pinning at impurity levels) of the origin of this semiconducting behaviour in a later section.

Figure 2c shows the typical I_{sd}–V_{bg} relationship obtained for the sample corresponding to Figure 2a when placed in atmospheric air for two weeks at room temperature. Because our fabricated GNRs are not covered with passivation films, the surfaces and edges of the GNRs are directly exposed to air and the edges are automatically oxidized through this process. We found that the initially observed n-type behaviour (Figure 2a) drastically changes to p-type behaviour (Figure 2c). The normalized I_{on}/I_{off} ratio (as large as ~10^6) observed in Figure 2b is also approximately observed in Figure 2d (with a logarithmic y-axis scale as in Figure 2b), although it is reduced by the larger leakage I_{sd}. Because the wider GNRs (~100 nm) showed no such change, this edge-sensitive characteristic is unique to the narrow (<20 nm) GNRs present. We confirmed qualitatively similar changes in five samples.

This is qualitatively consistent with the evident semiconducting behaviour observed in Figure 2a, and this result strongly suggests that the narrow GNRs' electronic structures are extremely sensitive to the termination of the dangling edge bonds by foreign atoms. It is known that the H-termination of GNR edges leads to electron doping and n-type behaviour [40], while O-termination by this process causes hole doping and p-type behaviour [41]. Evident changes between the n- and p-type behaviours in Figs. 2a and 2c may correspond to these edge terminations. Indeed, in the wider GNRs fabricated following the same CNT-derived method, p-type behaviour in an as-grown one and its transformation into ambipolar behaviour were reported after air-pumping in high vacuum for a long time [39]. This supports our results and the argument given above, although our narrow GNRs are much more sensitive to the atmosphere because the GNRs were only placed in air, without performing any intentional procedures. This result indicates that some portions of edge C–H bonds are chemically unstable and tend to be replaced by C=O bonds when the edges are exposed in air for a long time in the absence of covering passivation films. In the narrow and short GNRs (e.g., <20 nm width and <400 nm length), such a partial replacement can drastically change the electronic behaviours of all of the GNRs. The result also indicates that such GNRs are suitable for the fabrication of p- and n-type semiconducting devices via carrier doping from the edges and, hence, for CMOS-like circuits.

Figure 2e shows the typical I_{sd}–V_{bg} characteristics of ~3,600 nm-long GNRs (measured between electrodes 1 and 3 in Figure 1e) after O-termination of the edges by exposing the sample to atmospheric air. The curves indicate p-type

semiconducting behaviour, as in the case of Figure 2c. However, the onset value of V_{bg}, at which point I_{sd} starts to increase, is different in this case. The onset V_{bg} shifts to V_{bg} ~-4 V in Figure 2e. In contrast, the I_{sd}–V_{bg} relationship between electrodes 1 and 2 with a 400 nm distance on the same GNR (Figure 1e) is similar to that observed in Figure 2c, with the onset being V_{bg} = 0 V. These differences in the onset V_{bg} at the different portions of the long GNR can also be understood from the perspective of the poor uniformity of O-termination for the long GNR edges, as explained in a later section. This suggests that the electronic transport in narrow-width GNRs is highly sensitive not only to different types of foreign atoms but also to their quantities involved in edge termination.

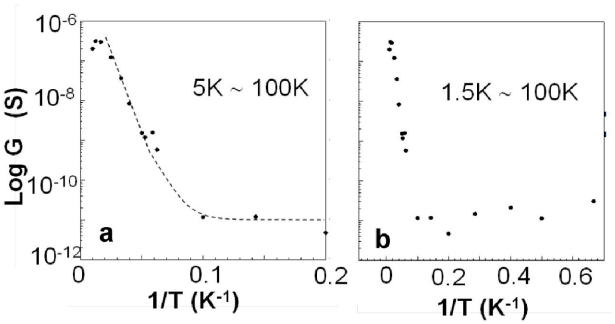

Figure 3. a, b, Arrhenius plots for the minimum conductance (G_{min}) vs. temperature of the sample corresponding to Figure 2a at T >5 K **(a)** and T >1.5 K **(b)**. The plotted G_{min} values were those obtained at V_{bg} = 0 V in Figure 2a. The dotted curve is just a visual guide.

This result also implies the possibility of fabricating GNR FETs with different threshold voltages by using different-length GNRs; this can prove useful in manufacturing LSI-circuit components using GNRs. In the LSI circuits, the tuning of the threshold voltages (current-onset voltage) is the most important. In the present experiments, the short GNRs with high homogeneous edge termination by the impurity atoms showed the lowest onset V_{bg}, while the long GNRs with inhomogeneous edge termination showed the highest onset V_{bg}. Thus, combining and hybridizing such different-length GNRs with different onsets of V_{bg} make the realization of LSI possible. Of course, the onset V_{bg} is not controllable in the present work, because only the unintentional termination of the edges was employed. If one could control it in the future, it would lead to the formation of an effective LSI circuit.

3.3 Small activation energy for impurity level

As mentioned, we have previously reported E_a values as large as ~50 meV in our fabricated wide GNRs, with minimum widths of ~75 nm. In order to compare the E_a value of the present narrow GNRs with the wide GNRs, we measured the relationship for minimum conductivity (G_{min}) vs. temperature for V_{bg} = 0 V in a few of the H-terminated n-type samples (Figure 2a). The corresponding Arrhenius plots are shown in Figure 3. The relationship is mostly linear when T >20 K, following a thermal-activation relationship as indicated by the dotted line, while the relationship is not clearly defined below T = 20 K, and the G_{min} value becomes extremely low while exhibiting a constant value when T <10 K (i.e., insulating behaviour). The linear part for T >20 K (the dotted line for1/T <0.05) yields E_a ~35 meV from fitting with $G_{min} \propto \exp(-E_a/2k_BT)$. Despite the narrow width of the GNRs (20 nm), this E_a value is less than the maximum E_a value of ~50 meV obtained for our previously-fabricated wider GNRs (minimum width ~75 nm), for which only the linear part was observed in the Arrhenius plots for the estimation of E_a.

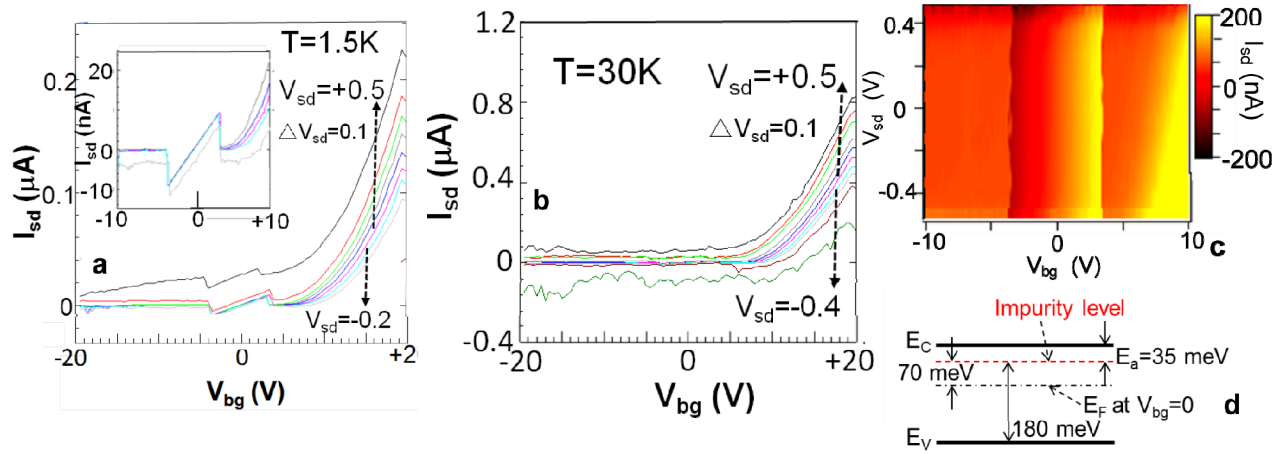

Figure 4. Conductance peaks at T = 1.5 K **(a)** and their disappearance at T = 30 K **(b)** in an H-terminated n-type short GNR. In (a), two evident conductance peaks are observed around V_{bg} = ±3.5 V. **Inset**: Magnification of the conductance peak shown in the main panel. **c**, V_{sd} dependence of the conductance peak. The *z*-axis represents I_{sd}. The yellow portions indicate high-I_{sd} regions. Two distinct vertical lines, which are attributed to the conductance peak, are observable around V_{bg} = ±3.5 V along the y-axis. **d,** Schematic band diagram for n-type behavior (Figure 2a). The activation energy E_a ~35 meV of the impurity level is estimated from the linear part of the curve shown in Figure 3a. The energy difference ~180 meV between the impurity level and the top of the valence band is also estimated from the V_{bg} region for the off-current (Figure 2a).

In general, the E_a value is inversely proportional to the GNR width W (i.e., $E_a = AW^{-1}$, where A denotes the coefficient). Although the A values were small in the previously-fabricated wide GNRs because of the large width region (W >75 nm), these low-defect GNRs exhibited large E_a values because of strong electron confinement in the clean 1D space of the low-defect GNRs [15]. This type of confinement should ideally be induced in the present narrower (W <20 nm) GNRs and, thus, the A value should increase. Moreover, the influence of armchair edges should become also significant in sub-10 nm-width GNRs. In our present near-sub-10 nm GNRs, such an influence should become non-trivial, thereby resulting in the enhancement of E_a. Nevertheless, the E_a observed in the present case is relatively smaller. This suggests that the anomalously small E_a value of ~35 meV is not characteristic of intrinsic energy band gaps. Because no power-law behaviour (i.e., $G_{min} \propto T^{\alpha}$ for hopping conductance) is observed even in the temperature regions where the linearity is smeared out (i.e., 10 K <T<20 K), the small value of E_a cannot be attributed to defect-originated energy levels, as in the case of lithographically fabricated GNRs [8-10].

On the other hand, it is known that the termination of GNR edges and carrier doping theoretically lead to the introduction of impurity levels

[35 - 39]. Indeed, this E_a value of ~35 meV estimated from Figure 3 is close to the impurity levels reported in [35]. The observed E_a value, thus, could be the activation energy of the electrons emitted from the impurity level to the bottom of the conduction band (Figure 4d) because of the measured V_{bg} = 0V.

3.4 Conductance peak at low V_{bg} fields

Here, in certain such small-E_a GNRs, we observe a sharp and small conductance peak in low V_{bg} regions (V_{bg} = ±3.5 V) of the I_{sd}–V_{bg} curves at T = 1.5 K (Figure 4a). Five of eight samples which showed the small E_a exhibited the conductance peaks. This suggests the strong correlation of the conductance peak with the impurity level with small E_a values. The conductance peak appears to be mostly independent of V_{sd} (Figure 4c). As the temperature increases, the conductance peak decreases and it disappears entirely at T ~30 K (Figure 4b). It can be, however, potentially the main cause for the abovementioned small E_a - which was observed at V_{bg} ~0 - over a wide temperature range in Figure 3(a).

When E_F is pinned around this impurity level, it can cause resonant tunnelling [35-37] and, thus, produce this sharp conductance peak. Here, in Figure 4(a), the conductance peaks exist around V_{bg} = ±3.5 V. This V_{bg} is the voltage applied from the back side of the silicon substrate and, thus, the applied V_{BG} modulates the electronic states of the GNRs via the silicon substrate, so electronic charging in the substrate ($Q_{BG} = C_{BG}\Delta V_{BG}$) gives rise to the true energy values [15].

Considering this, the energy in the single particle energy spectrum is given by $\Delta = (h/2\pi)\, v_F\sqrt{(2\pi C_{BG}\Delta V_{BG}/|e|)}$, where v_F ~10^6 m/s is the Fermi velocity of graphene and C_{BG} is the capacitive coupling of the GNR to the back-gate electrode. When C_{BG} is taken to be 230 aF μm^{-2}, which is 1/3 times smaller than that for our previous wide GNR [15], Δ for V_{bg} = 3.5 V in the present narrow GNRs is estimated to be ~70 meV. This means that the resonant tunnelling for the conductance peak occurs when E_F shifts in ~70 meV from the Dirac point at V_{bg} = 0V and is pinned by the impurity level.

We also discuss this issue in the next section, considering also other phenomena mentioned above.

Alternatively, carrier doping via edge termination by foreign atoms without considering the presence of impurity levels has been considered as the origin of the appearance of n- or p-type semiconductive behaviour, particularly in sub-10 nm-GNRs. However, in the present GNRs with ~20 nm widths, no 1D EDOS evidently exists because the width is >10 nm. Thus, the impurity levels with the small E_a ~35 meV introduced by edge termination can consistently explain the observed phenomena, as elucidated below (see Figure 4d).

3.5 Discussion

Theoretically, resonant tunnelling through the impurity levels theoretically produces conductance peaks [36,37]. Semiconducting ultra-narrow-armchair GNRs with impurities exhibited sharp peaks in DOS between VHSs as well as conductance due to resonant tunnelling, depending on the impurity concentration [36]. As the impurity concentration increased, the resonant-peak height increased. Moreover, the two connected GNRs with impurities also showed resonant tunnelling and conductance peaks, depending on the width of the GNRs and the hybridization energy of the impurity atoms in two GNRs [37].

As mentioned above, there is a strong correlation between the observed conductance peak and the impurity level with the small E_a value in the present, narrow GNRs. This suggests the robust possibility that the conductance peak originates from resonant tunnelling through the impurity level with an E_a value of ~35 meV, when E_F shifts ~70 meV from the Dirac point at V_{bg} = 0V and when E_F is pinned by the impurity level. Assuming this, all of the other three phenomena can be consistently understood qualitatively, as follows.

(1) The absence of transport gaps (Figure 2) can be understood by the model whereby E_F is strongly pinned around the high-intensity impurity level, which exists close to the bottom of the conduction band (E_a value of ~35 meV; Figure 4d) for H-terminated edges and close to the top of the valence band for O-terminated edges (Figure 2c; hole doping). The application of V_{bg}, thus, cannot shift E_F effectively through all the energy–regions present within the band gaps, resulting in the absence of transport gaps. (2) The high sensitivity upon the appearance of these n- and p-type behaviours to different atmospheres can also be understood by the closest position of E_F to the impurity level and the E_F pinning, especially for the present short GNRs (e.g., <500 nm length). The replacement of C-H bonds by edge C=O bonds can easily change the n-type behaviours to p-type behaviours due to the formation of high-intensity impurity levels in such short and narrow GNRs. (3) The large I_{on}/I_{off} value can also be explained by the model whereby drastic electron (hole) emissions can be caused due to the high-intensity of the impurity levels present, even upon slightly varying the applied V_{bg} and shifting the E_F. Indeed, I_{sd} rapidly increases right above V_{bg} = 0 V, both in Figs. 2b and 2d, resulting in the large I_{on}/I_{off} value. This is strong evidence for the E_F pinning model.

In the present narrow GNRs of width ~20 nm and length <~500 nm, the densities of the impurity levels will not be uniform through all the regions along the longitudinal direction because the termination by impurity atoms (H and O) is not uniform. It is speculated that some very small portions have the highest densities for tunnel barriers. When electrons run through such small tunnel barriers and V_{bg} is pinned by the impurity level, the electron must engage in resonant tunnelling. Moreover, the combination of two portions including the impurity levels in a GNR may correspond to the hybridization of the impurity level, like [37]. In this case, the emergence of a sharp conductance peak like that in Figure 5(a) can actually be predicted, depending on the hybridization energy. The models that are relevant to the present case should be clarified by further experiments.

Here, the difference in the onset V_{bg} value for different GNRs' lengths (Figs. 2c and 2e) can also be interpreted by poorer uniformity in the density of the impurity levels, caused by the occasional O-termination of the long GNR edges (i.e., the presence of extremely low-quantity C=O bonds at some edge sections). This is because the GNRs were unintentionally exposed to an air atmosphere.

The onset V_{bg} is determined by the energy difference between the initial position of E_F at V_{bg} = 0 V and the impurity levels. In the short GNRs, the edge-termination by H and O is relatively homogeneous with a high density. Thus, the impurity level density is high and homogeneous and hence the initial position of E_F locates close to the impurity level. Indeed, we estimated the initial position of E_F to be only 70 meV from the impurity level, as mentioned above. In contrast, in the unintentionally-oxidized long GNRs, some portions should have much lower O-termination and lower impurity levels as a matter of convention. In such portions, the initial E_F at V_{bg} = 0 V locates far from the impurity level according to the theory of semiconductors and, hence, the larger V_{bg} is needed in order to cause the onset to I_{sd}. The onset V_{bg} in the overall region of a long GNR is determined by such a portion, which has the largest resistivity. Therefore, the large onset V_{bg} appears in the long GNRs.

In Figure 2, I_{sd} cannot easily flow even under the applied maximum V_{bg} (i.e., V_{bg} = -20 V for Figure 2a and V_{bg} = +20 V for Figure 2c), except for the leaked I_{sd}. When we assume that E_F locates close to the impurity level at V_{bg} = 0 V and shifts directly following V_{bg} without undergoing pinning by the impurity level, we can estimate the energy difference Δ between the impurity level and the other band edges (i.e., the top of the valence band for the sample corresponding to Figure 2a and the bottom of the conduction band for that corresponding to Fig 2c). This energy difference can be also given by $\Delta = (h/2\pi)\, v_F\sqrt{(2\pi C_{BG}\Delta V_{BG}/|e|)}$ ~180 meV for the present GNR. This suggests that the energy band gaps Δ_{gap} of the present ~20 nm-wide GNRs are at least greater than [(Δ = 180) + (E_a = 35) meV = 215 meV]. This result is in qualitatively good agreement with the observed trend of GNR width vs. Δ_{gap} [15].

4. Conclusion

We reported on the unique semiconductive behaviours of narrow, low-defect GNRs, with widths of less than 20 nm. We found that the narrow GNRs were highly resistive and that additional annealing was required to reduce their resistivity. The GNRs did not show ambipolar but instead evident semiconductive behaviours (p- and n-types), exhibiting normalized I_{on}/I_{off} as great as ~10^6 (close to those in a few nm-order-width GNRs), which were very sensitive to the atmosphere and the termination of the GNR edges by foreign atoms (i.e., H atoms for n-type and O atoms for p-type). It was also anomalously revealed that the E_a (~35 meV) estimated from the temperature dependence of the minimum conductance was smaller than those in ~100 nm-width GNRs. The sharp conductance peak observed at low V_{bg} in the I_{sd}-V_{bg} curves exhibited a strong correlation with the presence of shallow impurity levels with the small E_a, which were introduced by the edge terminations by H atoms. This possibly originated from resonant tunnelling via the pinning of E_F by the impurity level, which provided the observed, unique semiconducting behaviour. An energy

band gap as large as ~215 meV was also confirmed from the I_{sd} off-voltage region on V_{bg}.

The narrow GNRs fabricated in this study are suggestive of the utility of high-efficiency semiconducting graphenes bearing edges terminated by a variety of hetero-atoms. The FETs prepared with such GNRs can lead to the fabrication of efficient graphene LSI circuits based on CMOS-like operations, because they easily provide for n- and p-type semiconducting behaviours as well as different onset voltages. As other unique applications of graphenes, nanoresonators (e.g., utilizing the enhanced mass-sensitivity due to the effective strain in the non-linear oscillation [42] as well as the unique lattice dynamics' properties in twisting bilayer graphene [43]) have recently been proposed. Moreover, it was predicted that ZnO nanowire without polar surfaces can exhibit high thermal conductivity [44]. The present, very thin GNRs, may also be good candidates for such applications. Moreover, the introduction of spin-orbit interaction [45] and the utilization of edge-polarized spins [29-31] in the present thin GNRs must open the door to novel spintronic devices.

5. Acknowledgements

The authors thank Y. Iye, S. Katsumoto, Y. Hashimoto, A. Endo, S. Tarucha, M. Yamamoto, T. Ando, T. Enoki, X. M. Jia, and M. S. Dresselhaus for technical support, fruitful discussions, and encouragement. The work at Aoyama Gakuin was partly supported by a Grant-in-Aid for Scientific Research in MEXT and grant for AFOSR.

6. References

[1] Novoselov KS, Geim AK, Morozov SV, Jiang D, Zhang Y, Dubonos SV, Grigorieva IV and Firsov AA (2004) Electric field effect in atomically thin carbon films. Science 306: 666–669.

[2] Geim AK and Novoselov KS (2007) The rise of graphene, Nature Mater. 6: 183–191.

[3] Zhao Y, Cadden-Zimansky P, Jiang Z and Kim P (2010) Symmetry breaking of the zero energy Landau level in bilayer graphene. Phys. Rev. Lett. 104: 066801.

[4] Zhang YB, Tang TT, Girit C, Hao Z, Martin MC, Zettl A, Crommie MF, Shen YR and Wang F (2009) Direct observation of a widely tunable bandgap in bilayer graphene. Nature 459: 820–823.

[5] Craciun MF, Russo S, Yamamoto M, Oostinga JB, Morpurgo AF and Tarucha S (2009) Trilayer graphene is a semimetal with a gate-tunable band overlap. Nature Nanotech. 4: 383–388.

[6] Park J, Jo SB, Yu YJ, Kim Y, Yang W, Lee WH, Kim HH, Hong BH, Kim P, Cho K and Kim KS (2012) Single-gate bandgap opening of bilayer graphene by dual molecular doping. Adv. Mater. 24: 407-411.

[7] Yang JW, Lee G, Kim JS and Kim KS (2011) Gap opening of graphene by dual FeCl3-acceptor and K-donor doping. J. Phys. Chem. Lett. 2: 2577-2581.

[8] Han MY, Brant JC and Kim P (2010) Electron transport in disordered graphene nanoribbons. Phys. Rev. Lett. 104: 056801.

[9] Stampfer C, Guttinger J, Hellmueller S, Molitor F, Ensslin K and Ihn T (2009) Energy gaps in etched graphene nanoribbons. Phys. Rev. Lett. 102: 056403.

[10] Cresti A and Roche S (2009) Edge-disorder dependent transport length scales in graphene nanoribbons: from Klein defects to the superlattice limit. Phys. Rev. B 79: 233404.

[11] Evaldsson M, Zozoulenko IV, Xu HY and Heinzel T (2008) Edge-disorder-induced Anderson localization and conduction gap in graphene nanoribbons. Phys. Rev. B 78: 161407.

[12] Mucciolo ER, Castro Neto AH and Lewenkopf CH (2009) Conductance quantization and transport gaps in disordered graphene nanoribbons. Phys. Rev. B 79: 075407.

[13] Lherbier A, Biel B, Niquet YM and Roche S (2008) Transport length scales in disordered graphene-based materials: strong localization regimes and dimensionality effects. Phys. Rev. Lett. 100: 036803.

[14] Yang L, Park CH, Son YW, Cohen ML and Louie SG (2007) Quasiparticle energies and band gaps in graphene nanoribbons. Phys. Rev. Lett. 99: 186801.

[15] Shimizu T, Haruyama J, Marcano DC, Kosinkin DV, Tour JM, Hirose K, Suenaga K (2011) Large intrinsic energy bandgaps in annealed nanotube-derived graphene nanoribbons. Nat. Nanotech. 6: 45–50.

[16] Kosynkin DV, Higginbotham AL, Sinitskii A, Lomeda JR, Dimiev A, Price BK and Tour JM (2009) Longitudinal unzipping of carbon nanotubes to form graphene nanoribbons. Nature 458: 872–876.

[17] Higginbotham AL, Kosynkin DV, Sinitskii A, Sun, ZZ and Tour JM (2010) Low-defect graphene oxide nanoribbons from multiwalled carbon nanotubes. ACS Nano 4: 2059–2069.

[18] Jiao L, Wang XR, Diankov G, Wang HL and Dai HJ (2010) Facile synthesis of high-quality graphene nanoribbons. Nature Nanotech. 5: 321–325.

[19] Li XL, Wang XR, Zhang L, Lee SW and Dai HJ (2008) Chemically derived, ultrasmooth graphene nanoribbon semiconductors. Science 319: 1229–1232.

[20] Wang X, Ouyang Y, Li X, Wang H, Guo J and Dai H (2008) Room-temperature all-semiconducting sub-10-nm graphene nanoribbon field-effect transistors. Phys. Rev. Lett. 100: 206803.

[21] Rangel NL, Sotelo JC and Seminario JM (2009) Mechanism of carbon nanotubes unzipping into graphene ribbons. J. Chem. Phys. 131: 031105.

[22] Son YW, Cohen ML and Louie SG (2006) Energy gaps in graphene nanoribbons. Phys. Rev. Lett. 97: 216803.

[23] Son YW, Cohen ML and Louie SG (2006) Half-metallic graphene nanoribbons. Nature 444: 347–349.
[24] Nakada K, Fujita M, Dresselhaus G and Dresselhaus MS (1996) Edge state in graphene ribbons: Nanometer size effect and edge shape dependence. Phys. Rev. B 54: 17954-17961.
[25] Castro Neto AH, Guinea F, Peres NMR, Novoselov KS and Geim AK (2009) The electronic properties of graphene. Rev. Mod. Phys. 81: 109–162.
[26] Kim WY and Kim KS (2008) Prediction of very large values of magnetoresistance in a graphene nanoribbon device. Nat. Nanotech. 3: 408-412.
[27] Min SK, Kim WY, Cho Y and Kim KS (2011) Fast DNA sequencing with a graphene-based nanochannel device. Nat. Nanotech. 6: 162-165.
[28] Mencarelli D and Pierantoni L (2012) Analysis of the metal work function dependence of charge transfer in contacted graphene nanoribbons. Nanomater. Nanotechnol. 2: 12. doi: 10.5772/54995
[29] Tada K, Hashimoto T, Haruyama J, Yang H and Chshiev M (2012) Spontaneous spin polarization and spin pumping effect on edges of graphene antidot lattices. Phys. Status Solidi B 249: 2491–2496.
[30] Shimizu T, Nakamura J, Tada K, Yagi Y and Haruyama J (2012) Magnetoresistance oscillations arising from edge-localized electrons in low-defect graphene antidot-lattices. Appl. Phys. Lett. 100: 023104.
[31] Hashimoto T, Kamikawa S, Yagi Y and Haruyama J (2014) Electronic properties of nanopore edges of ferromagnetic graphene nanomeshes at high carrier densities under ionic-liquid gating, Materials Sciences and Applications 5: 1-9.
[32] Jia X, Hofmann M, Meunier V, Sumpter BG, Campos-Delgado J, Romo-Herrera JM, Son H, Hsieh Y, Reina A and Kong J (2009) Controlled formation of sharp zigzag and armchair edges in graphitic nanoribbons. Science 323: 1701–1705.
[33] Girit ÇÖ, Meyer JC, Erni R, Rossell MD, Kisielowski C, Yang L, Park C, Crommie MF, Cohen ML and Louie SG (2009) Graphene at the edge: stability and dynamics. Science 32: 1705–1708.
[34] Bai J, Zhong X, Jiang S, Huang Y and Duan X (2010) Graphene nanomesh. Nat. Nanotech. 5: 190–194.
[35] Sieranski K and Szatkowski J (2013) The energies of the substitutional impurities in graphene. Phys. Status Solidi B 250: 1556–1562.
[36] Zhou BL, Zhou BH, Chen XW and Zhou GH (2012) Electronic transport for impurity-doped armchair-edge graphene nanoribbons. Eur. Phys. J. B 85: 121.
[37] Belonenko MB, Pak AV and Lebedev NG (2013) Tunneling current of the contact between impurity-containing graphene nanoribbons. Semiconductors 47: 662–664.
[38] Qiu W and Skafidas E (2013) Quantum conductance of armchair graphene nanopores with edge impurities. J. Appl. Phys. 114: 073703.
[39] Sinitskii A, Dimiev A, Kosynkin DV and Tour JM (2010) Graphene nanoribbon devices produced by oxidative unzipping of carbon nanotubes. ACS Nano 4(9): 5405–5413.
[40] Kim BH, Hong SJ, Baek SJ, Jeong HY, Park N, Lee M, Lee SW, Park M, Chu SW, Shin HS, Lim J, Lee JC, Jun Y and Park YW (2012) N-type graphene induced by dissociative H2 adsorption at room temperature. Scientific Reports 2: 690, DOI: 10.1038 /srep00690.
[41] Ouyang Y, Sanvito S and Guo J (2011) Effects of edge chemistry doping on graphene nanoribbon mobility. Surface Science 605: 1643–1648.
[42] Jiang JW, Park H and Rabczuk T (2013) Polar surface effects on the thermal conductivity in ZnO nanowires: a shell-like surface reconstruction-induced preserving mechanism. Nanoscale 5: 11035.
[43] Jiang JW, Park HS, Rabczuk T (2012) Enhancing the mass sensitivity of graphene nanoresonators via nonlinear oscillations: the effective strain mechanism. Nanotechnology 23(47): 475501.
[44] Jiang JW, Wang BS and Rabczuk T (2012) Acoustic and breathing phonon modes in bilayer graphene with Moiré patterns. Appl. Phys. Lett. 101(2): 023113.
[45] Balakrishnan J, Koon GKW, Jaiswal M, Castro Neto AH and Özyilmaz B (2013) Colossal enhancement of spin–orbit coupling in weakly hydrogenated graphene. Nature Physics 9: 284-287.

7. Author's note

The temperature dependence of the G_0 anomaly (Figure 1f) does not follow the expression for the single-electron charging (SEC) effect [13]. SEC is caused by a charging energy of single electron ($E_c = e2/2C$, where C is the capacitance of the dot) confined into quantum dot isolated by two tunnel barriers. Current cannot flow at the voltages $<E_c/e=e/2C$ (i.e., G_0 anomaly) because of the so-called Coulomb blockade. In the conventional GNR, the GNR should be this quantum dot and the two barriers should correspond to the two interface barriers between the GNR and two metal electrodes (i.e., source and drain). In contrast, when the ends of CNTs or GNRs are covered by metal electrodes and have electrical contacts (the so-called end bonding), the interface resistivity becomes very low and tunnel barriers do not exist mostly, leading to disappearance of SEC and G_0 anomaly. We formed this end-bonding structure on the present GNRs (Figure 1d) and, thus, the observed G_0 anomaly should not come from the SEC effect.